

Electrical breakdown in Thick-GEM based WELL detectors

A. Jash^{a,1} **L. Moleri,**^a **S. Bressler**^a

^a*Department of Particle Physics and Astrophysics, Weizmann Institute of Science, Herzl st. 234, Rehovot 7610001, Israel*

E-mail: abhik.jash@weizmann.ac.il

ABSTRACT: Occurrence of electrical breakdown (i.e. discharges) in gas detectors restrict their dynamic range and degrade their performance. Among the different methods developed to mitigate these effects, the use of resistive materials in the detector assembly has been found to be very effective. In this paper, we studied and characterized electrical discharges in Thick-GEM based WELL-type detectors with and without resistive elements. We present a new method to measure discharges in the resistive configurations which allows demonstrating for the first time the occurrence of discharges in the Resistive Plate WELL detector as well. It also provides a direct measurement of the Raether limit.

KEYWORDS: Micropattern gaseous detectors (MSGC, GEM, THGEM, RETHGEM, MHSP, MICROPIC, MICROMEGAS, InGrid, etc), Gaseous detectors; Electron multipliers (gas), Resistive-plate chambers

¹Corresponding author.

Contents

| | | |
|----------|---|-----------|
| 1 | Introduction | 1 |
| 2 | Experimental setup and Methodology | 3 |
| 2.1 | WELL structures | 3 |
| 2.2 | Setup | 3 |
| 2.3 | Methodology | 4 |
| 3 | Results | 9 |
| 4 | Summary | 11 |
| A | RPWELL gain curves at different source rates | 12 |

1 Introduction

Micro-Pattern Gas Detectors (MPGDs) are candidates of choice for many ongoing and future experiments due to their excellent spatial and energy resolutions, high detection efficiency, high rate capabilities and the potential of being industrially produced. Nonetheless, the dynamic range of MPGDs is often limited by the occurrence of occasional discharges that could result in efficiency loss, damage to the detector electrodes and to the readout electronics.

The sequence of events leading to a discharge is initiated when the avalanche size (product of primary ionization and gain) exceeds a few 10^7 ion-electron pairs, the so-called Raether limit [1]. The resulting modification of the local field becomes large enough to induce a transition of the avalanche to a forward–backward propagating streamer, a well-studied process (see for example [1–3]). Due to the small distance between the electrodes in MPGDs, the streamer is likely to form an electrical connection between nearby electrodes of different potentials, consequently discharging the energy stored in the equivalent capacitor.

Different methods were developed to resolve the problem of discharges; in cascade structures [4, 5] the electric field in each charge multiplication stage is weaker such that larger charge density is needed in order to trigger a discharge and higher gains could be reached. The usage of finer detector segmentation [6] do not allow reaching higher gains, instead it reduces the area affected by a discharge, and the corresponding discharge energy stored in the equivalent capacitor. In recent years, the most common approach for mitigating discharges in MPGDs is embedding resistive electrodes in the detector assembly [7, 8]. This has two roles: (i) Protecting the readout electronics by decoupling it from the energy released in the discharge of the effective capacitor. (ii) Quenching the discharge energy. As shown for Resistive Plate Chambers [9], the long clearance time of charges from the resistive material results in a local self-reduction of the electric field and self-extinction of the discharge.

In the present work, we study discharges in three different THGEM-based WELL detectors: standard THick-WELL (THWELL) [10] with no resistive material embedded, Resistive-WELL (RWELL) [11], and Resistive Plate WELL (RPWELL) [12]. We demonstrate the effect of the resistive materials on various discharge characteristics.

The THGEM electrode [13, 14] is a scaled-up (~tenfold) variant of the Gas Electron Multiplier (GEM) [15] foil. Typical electrodes are produced by standard printed-circuit board (PCB) technology: mechanical drilling of sub-millimeter diameter hole pattern through insulating (e.g. FR4) plates copper-clad on both sides followed by chemical etching of concentric insulating rims around the hole edges (the latter were found to considerably reduce the discharge probability, at the cost of some charging up effects [16, 17]). The Thick WELL electrode is copper-clad on one side only.

THGEM detectors are suitable for applications requiring large area coverage at sub-mm spatial resolution [18, 19], a few ns time resolution [20], high counting rate capability [21] and robustness against occasional discharges [22].

In a standard THGEM detector configuration, the THGEM electrode is preceded by a conversion and drift gap. Radiation-induced ionization electrons drift into the THGEM holes, where multiplication occurs under a high electric field. The resulting avalanche electrons are extracted into a few-mm wide induction gap and drift towards the readout anode, inducing a signal.

In a THWELL detector configuration (figure 1a), the single-sided THGEM electrode is coupled directly to the anode. The absence of the induction gap leads to a significantly thinner geometry - an advantage for applications with stringent space limitations [23]. Compared to a THGEM with an induction gap, higher gains could be obtained for lower applied voltage across the THGEM electrode, due to the larger electric field within the closed holes [24]. Signals are induced on the readout anode by the movement of avalanche electrons and ions inside the holes.

In the resistive-WELL (RWELL) detector [11] (figure 1b), the THGEM WELL-electrode is coupled to the readout anode through a resistive layer. The latter is deposited on an insulating sheet. This configuration was proposed in an attempt to protect the multiplier, its anode and the readout electronics from discharge damages and to minimise eventual dead-time effects following a discharge. Using resistive material of $10 \text{ M}\Omega/\square$, it was shown that while the discharge probability remains similar to that of a THWELL configuration [10], the energy released during a discharge is, indeed, quenched by an order of magnitude.

In the Resistive-Plate WELL (RPWELL) [12] detector (figure 1c), the WELL electrode is coupled to the readout anode through a material of high bulk resistivity ($\sim 10^9 - 10^{12} \text{ }\Omega\text{cm}$). Compared to the RWELL, this geometry has higher resistivity which should provide superior discharge protection and quenching. Indeed, in earlier works [12, 25–27], in which discharges were defined as large ($\sim 10 \text{ nA}$) current fluctuations, the RPWELL has always been treated as a discharge free detector. In the present work, we demonstrate the appearance of discharges in RPWELL detectors as well and characterize them relative to discharges occurring on the THWELL and RWELL configurations.

This paper is organized as follow: in section 2, we describe the investigated detector configurations, the experimental setup and the methodology used. The results comparing the three configurations in terms of discharge intensity and probability are presented in section 3, followed by a discussion in section 4.

2 Experimental setup and Methodology

2.1 WELL structures

For all the studied configurations, a 0.4 mm thick single-faced THGEM with $20\text{ mm} \times 20\text{ mm}$ active area is used. It has 0.5 mm diameter holes with 0.1 mm rim, arranged in a square pattern with 1 mm pitch. An Aluminum mesh is used as cathode and is placed 3 mm above the THGEM. The mesh allows the passage of low energy X-rays for the characterization purpose. The three WELL-based detectors are described below.

1. **THWELL** - the single-sided THGEM is directly coupled to the metallic anode (figure 1a).
2. **RWELL** - a mixture of graphite and lacquer providing a surface resistivity of $16\text{ M}\Omega/\square$ was sprayed on 0.9 mm (0.2 mm) thick FR4 plate. This layer was placed between the THGEM and the anode with its graphite-painted side facing to the THGEM (figure 1b). To allow charge evacuation through the graphite layer one of its edges was connected to the ground by a copper line.
3. **RPWELL** - a 0.7 mm thick LRS glass [28] with bulk resistivity $2 \times 10^{10}\text{ }\Omega\text{cm}$ is placed in between the THGEM and anode (figure 1c). The bottom of the resistive glass is attached to the anode using a conductive tape to ensure good electrical contact between the two.

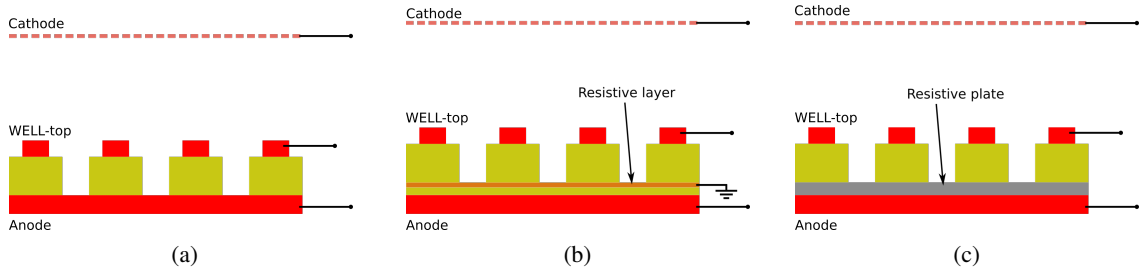


Figure 1: Schematic diagram (not to scale) and bias scheme of the three detector types: (a) THWELL, (b) RWELL, (c) RPWELL.

2.2 Setup

A schematic diagram of the experimental setup is shown in figure 2 with RWELL as a representative detector. A similar scheme is followed for the THWELL and RPWELL. A gas mixture containing 95% Neon and 5% CH_4 is continuously flown at 20 cc per minute through the chamber at atmospheric pressure. The detectors are irradiated using X-rays from a Cu-target X-ray generator (model: Oxford instruments 5500). A few μm thick Nickel filter placed in the path of the X-rays suppresses low energy Bremsstrahlung photons and allows the ones corresponding to the K_α peak of Cu (8.04 keV energy). A 20 cm long Aluminium tube with 0.5 mm diameter opening was used to collimate the X-ray beam. The rate of the X-ray source was set by the current flowing through the X-ray generator tube, operated at 30 kV.

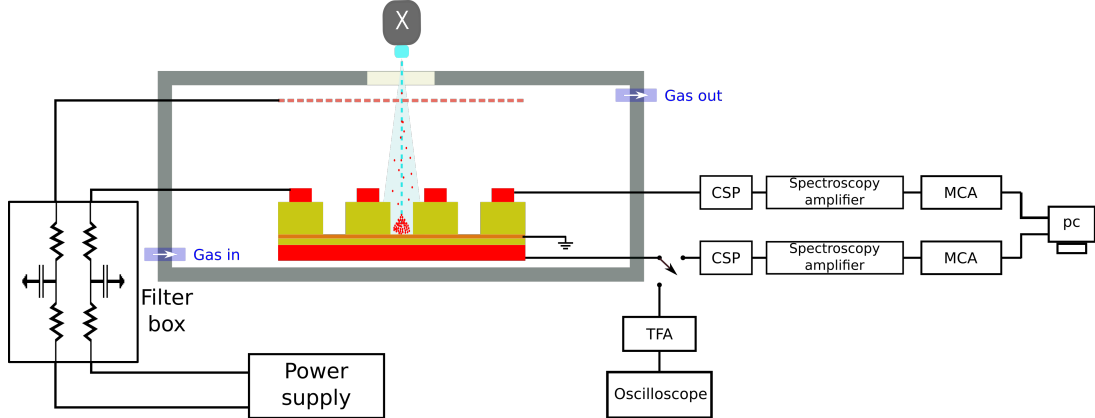


Figure 2: Schematic diagram of the detector assembly (not to scale).

The Well-top and the cathode are biased using a CAEN N1471 power supply via a low pass filter and a $10\text{ M}\Omega$ decoupling resistor, so that the capacitance in the filter does not add to the discharge. The anode is maintained at ground potential. It is connected to either the electronic chain with charge sensitive pre-amplifier (CSP) (model: CANBERRA 2006), spectroscopic amplifier (model: ORTEC 471), Multi-Channel Analyzer (MCA) (model: Amptek 8000D), or to the chain with the timing-filter amplifier (TFA) (model: ORTEC 474) and oscilloscope (model: Keysight DSOX3034A), depending on the requirement. The CSP signals are shaped using a spectroscopic amplifier to cut the long tail which gives rise to event pile-up. The case-specific connections will be described in section 2.3. The Well-top is biased (bias voltage denoted as V_{WELL}) via a charge sensitive pre-amplifier (model: ORTEC 142) to allow reading out signals from the top electrode as well. The Well-top signal after the pre-amplifier is connected to a spectroscopic amplifier (model: CAEN N968) and then to an MCA (model: Amptek 8000D).

2.3 Methodology

Upon assembly of a detector setup and prior to any measurement the system was flushed with the Ne/5% CH_4 gas mixture for 1 hour at 20 cc per minute, corresponding to three volume changes. Then the electrodes were biased and the X-ray source was switched on to irradiate the detector. This was followed by a 12 hours waiting period to ensure gain stabilization [16, 17]. Likewise, we waited for 30 minutes after any change in voltage.

Gain characterization: The first step of the study involved basic characterization of the detector in terms of charge spectrum and gain curve. The results were taken as reference and used to decide the operating conditions for the discharge studies. To obtain the charge spectra, the anode is connected to the electronic chain of CSP, spectroscopic amplifier, MCA. The MCA distribution is converted to the corresponding charge by calibrating it using a known value of input charge. The calibrated MCA spectra from the anode of the three detectors at an applied voltage, $V_{WELL} = 700$ V are shown in figure 3a. As can be seen, at the same voltage (700 V), the total induced charge in RWELL with 0.9 mm thick FR4 is significantly lower than the other two detectors which had similar spectra.

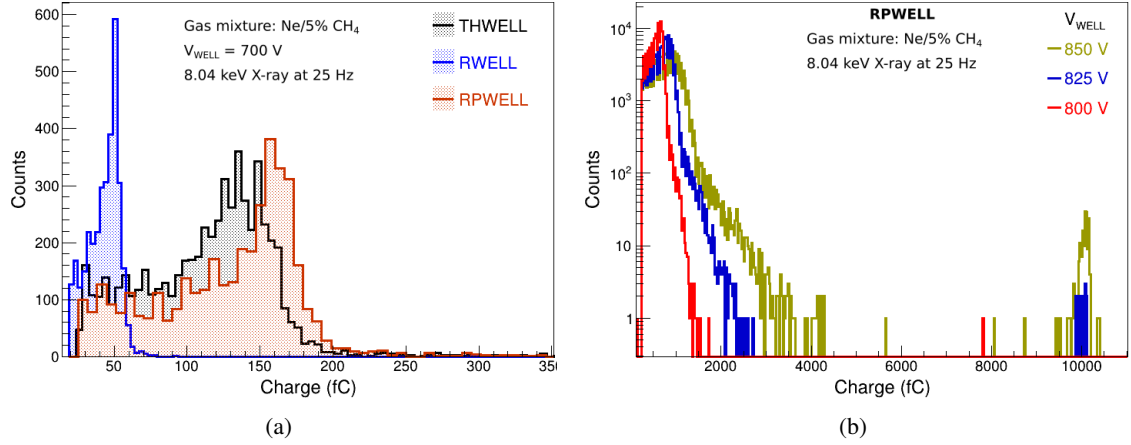


Figure 3: (a) Calibrated MCA spectra from the three detectors at $V_{WELL} = 700$ V, (b) MCA spectra of RPWELL at higher voltages showing a second population corresponding to saturation of CSP produced by discharges. The counts in the second population increases with voltage.

The effective gain was calculated by dividing the integrated charge induced on the readout anode by the primary charge produced by the incident radiation. The induced charge is extracted from the MCA spectra, which show a distribution with a peak corresponding to 8.04 keV X-rays. The corresponding average number of primary electrons produced in Ne/5% CH₄ calculated using HEED [29] is 229 corresponding to a primary charge of about 0.04 fC. The effective gain of the three detectors calculated at different applied voltages is shown in figure 4 for the lowest radiation X-ray rate corresponding to around 25 Hz acquisition rate. At any voltage the effective gains of

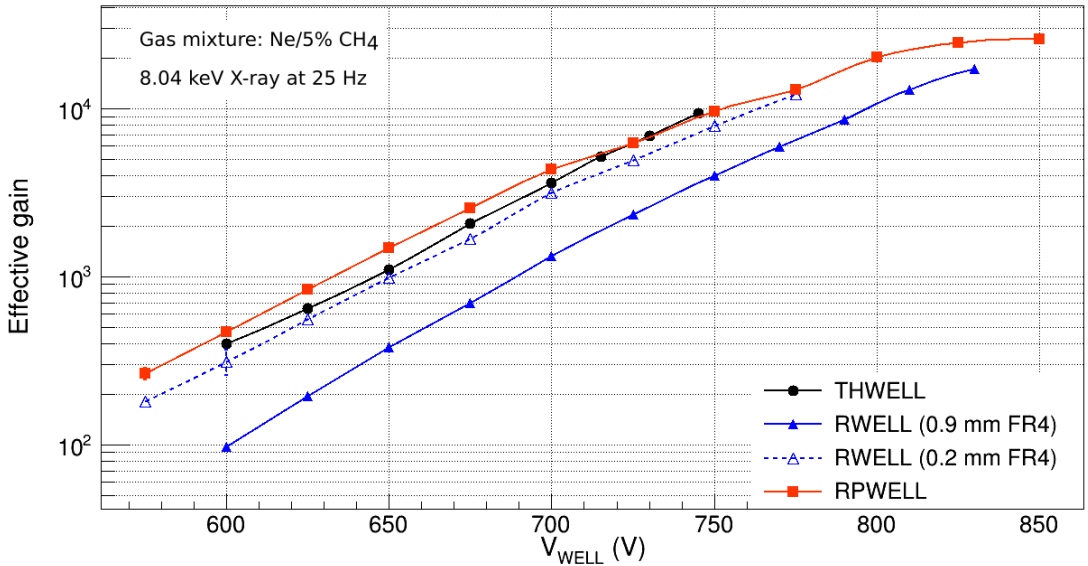


Figure 4: Variation of effective gain of the investigated detectors with the applied voltage at a source rate of 25 Hz.

THWELL and RPWELL were found to be close whereas a significantly lower gain was observed for the RWELL with 0.9 mm FR4. To understand the lower gain in RWELL which is inconsistent with the previously reported results [10, 27], the measurement was repeated with a RWELL with a thinner (0.2 mm) FR4 and the gain curve was found to be close to the other two detectors and in consistency with the past publications. The low gain in the RWELL with thicker FR4 can be understood from the Shockley-Ramo theorem [30, 31] which states that the magnitude of induced current on a readout electrode is proportional to the weighting field vector of that electrode. Simulation of the weighting fields in the two RWELL geometries with thick and thin insulator layers showed a two times higher value in the thinner RWELL, which can explain the observed gain values. The same logic does not necessarily fit the RPWELL case. Unlike the FR4 layer in the RWELL, electrons can move inside the resistive material which can not be simulated as a perfect insulator. Indeed, as seen in figure 4 and as reported in [12], the addition of a resistive plate has small effect on the measured charge and corresponding effective gain. The RWELL results reported later in this paper are for the one with 0.9 mm FR4.

Similar to other MPGDs, the effective gain of THWELL structures increases exponentially with the applied voltage. A maximum gain of about 9.5×10^3 can be achieved in THWELL at $V_{WELL} = 745$ V above which the production of strong discharges at high rate prohibit the detector operation. The RWELL detector can be operated at a higher maximum achievable gain of about 2×10^4 at $V_{WELL} = 830$ V, above which discharges prohibit its operation. For the RPWELL, though discharges from the monitored power supply currents were not observed even at relatively high voltage values, events with large charge content saturating the CSP appeared. It can be observed as an additional population in the MCA spectrum of RPWELL around 10000 fC charge in figure 3b. The rate of large pulses increases with voltage. The RPWELL gain curve was found to deviate from exponential nature and a saturating behavior was observed towards the end of the curve. A maximum gain of about 3×10^4 was achieved at 850 V, above which the acquired spectra were distorted.

The effective gain of RPWELL has a strong dependence on the radiation rate [12]. It is discussed in detail in appendix A. To minimize the effects due to source rate, all the measurements were performed at the lowest possible source rate corresponding to 25 Hz MCA acquisition rate.

Discharge characterization from power supply currents: The standard method of discharge identification in a gas detector relies on the observation of sudden currents supplied to the participating electrodes. The power supply current monitor of all the channels was digitized using NI USB-6008 DAQ with Signal Express software at a sampling rate of 2 kHz. In normal operating conditions the electrode currents show zero value from all the electrodes in all the investigated detectors. The current measured along 5 minutes on all the THWELL detector electrodes is shown in figure 5a at $V_{WELL} = 745$ V where discharges appear occasionally. The positive Well-top current is accompanied by simultaneous negative current on the anode, implying flow of current between these two electrodes during the discharge. Pile up of these spikes is present from time to time, indicating a possible multiple discharge event. The large current is accompanied by significant (up to 20 V) voltage drop observed in the power supply. The recovery time (2 seconds in the present case) is a property of the power supply itself.

The electrode currents measured in the RWELL in presence of discharges are shown in figure

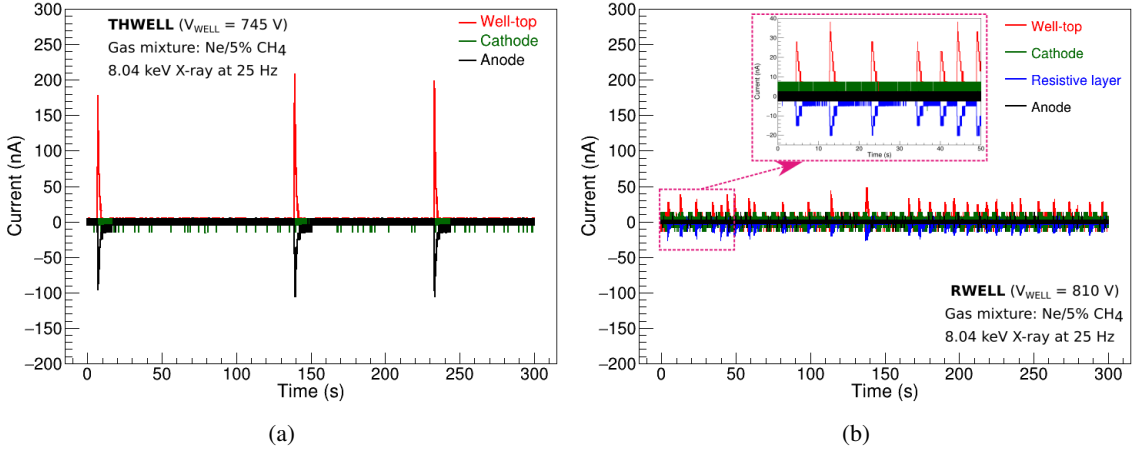


Figure 5: The monitored supplied currents to all the electrodes of (a) a THWELL at $V_{WELL} = 745$ V, (b) a graphite RWELL at 810 V (zoomed view in the inset) with an effective gain around 10^4 .

5b. Occurrence of a discharge shows current spikes similar to the one observed with the THWELL, but the opposite polarity spikes are measured on the Well-top and resistive layer (instead of the anode). As shown also in [10], the amplitude of the current spikes is lower compared to that measured in a THWELL operated at the same gain (figure 5a), demonstrating the effect of the resistive layer in quenching the discharge. The similar behavior between THWELL and RWELL points to the fact that the discharge mechanism is the same. For both detectors we could measure the discharge intensity as the total charge produced, i.e. the integral of the power supply current spike.

The current fluctuations due to discharges in the RPWELL configurations were at the order of hundreds of pA to a few nA. While they were visible on the power supply controller screen, they were below the sensitivity of the NI-DAQ recording system. Due to the limited sensitivity, the RPWELL detector was described as "discharge-free" in previous publications.

Discharge characterization from induced signals: We used the electronic chain with TFA and oscilloscope to monitor the anode pulses with minimum shaping with 10 ns integration time and 150 μ s differentiation time. A typical avalanche signal from THWELL anode at normal operating condition, amplified by the TFA is shown in figure 6a. The electrons (ions) produced in an avalanche drift towards the anode (Well-top) and induce a negative (positive) signal of a few mV amplitude. The \sim 50 ns rise time is attributed to the fast motion of electrons [32]. The \sim μ s tail is due to the slower motion of ions away from the anode.

In THWELL, RWELL and RPWELL, the avalanche induced anode signals have similar shape [12]. In the RWELL, an additional low-current was measured on the resistive layer. A typical case is shown in figure 6b where the anode signal is amplified by the TFA and the resistive layer one is integrated by the CSA. Considering the polarity inversion in the CSP, we see the signals from anode and resistive layer are of same polarity. The slow rise of this pulse indicates that it originates from the slow evacuation of the deposited electrons in the graphite layer to ground, which has two main effects on the detector performance. During a gas breakdown, a large amount of charges

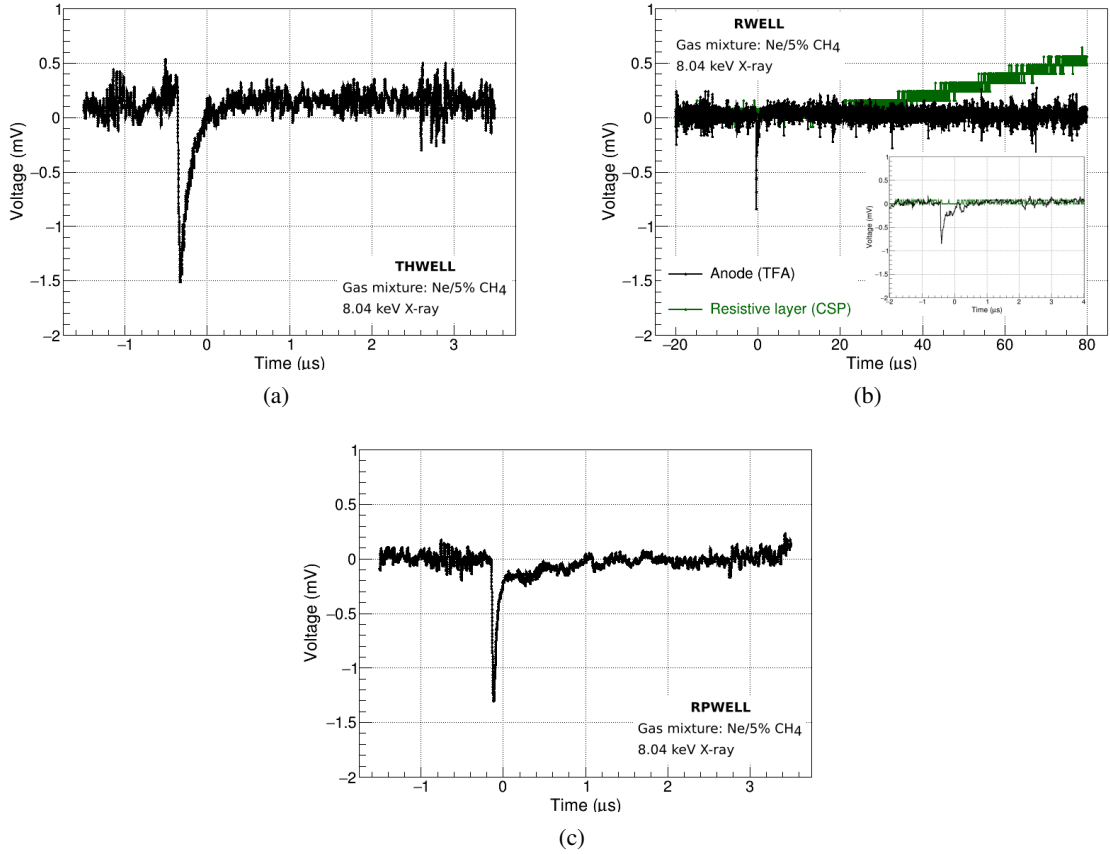


Figure 6: Typical avalanche-like signals from a (a) THWELL anode, (b) RWELL anode and resistive layer, (c) RPWELL anode. The anode signals are amplified by a timing filter amplifier with 10 ns integration time and the signal from resistive layer is inverted and integrated by a charge-sensitive preamplifier.

accumulate locally, causing a field reduction, and consequently quenching the discharge energy. Also, the charge movement in the resistive material causes a voltage drop along its path to ground. This is the cause of the rate dependence of the gain of resistive detectors.

Around their maximal operation voltages (in the discharge regime), high-amplitude signals of order of a few hundreds of mV are induced on the RWELL and RPWELL anodes. In the RWELL, these pulses are correlated with discharges identified by power supply current spikes. A typical high-charge pulse is shown in figure 7a. In the case of RPWELL, the appearance of these large-amplitude pulses is correlated with a tiny current fluctuation in the WELL-top power-supply current (up to a few nA). A typical induced pulse for a discharge-like event in RPWELL is shown in figure 7b. Discharges occurring at the THWELL saturate the TFA (input range ± 1 V) and no meaningful signal could be acquired.

The high-amplitude pulses were used to trigger on discharge events in the two resistive configurations. The amplitude of these discharge-like pulses was measured using the oscilloscope (with 50Ω input impedance). It was calibrated to charge following the method described in [33].

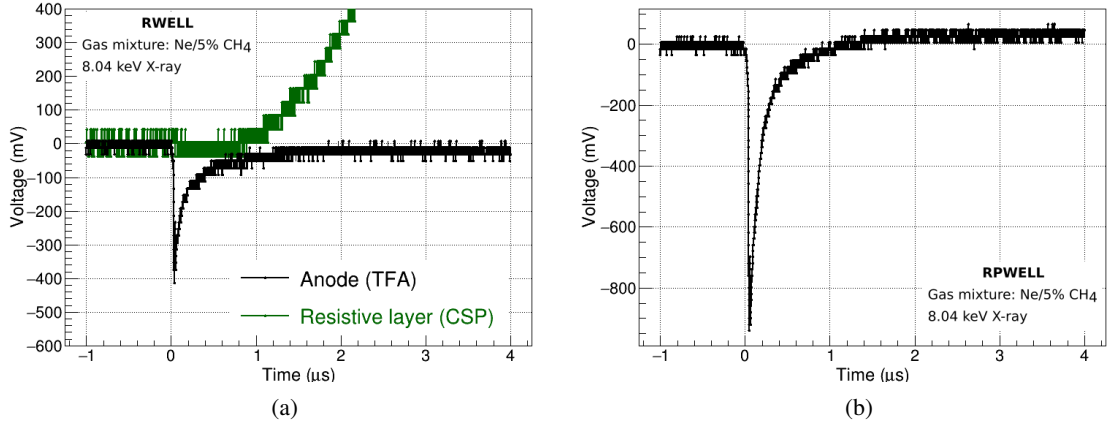


Figure 7: Typical discharge-like signal from a (a) RWELL anode, (b) RPWELL anode after a timing filter amplifier with 10 ns integration time.

For the three detector configurations, the discharge probability was estimated as the number of discharges acquired over the acquisition time and source rate.

3 Results

Following the methodology discussed in detail in section 2.3, the pulses induced on the RWELL and RPWELL anode were measured with the TFA. The equivalent charge was estimated from the pulse heights. The charge distribution is shown for the RWELL and RPWELL in figures 8a and 8b, respectively. In both figures, two populations separated by three orders of magnitude are clearly observed. The first (black curve) corresponds to the normal, avalanche-like, pulses. These pulses

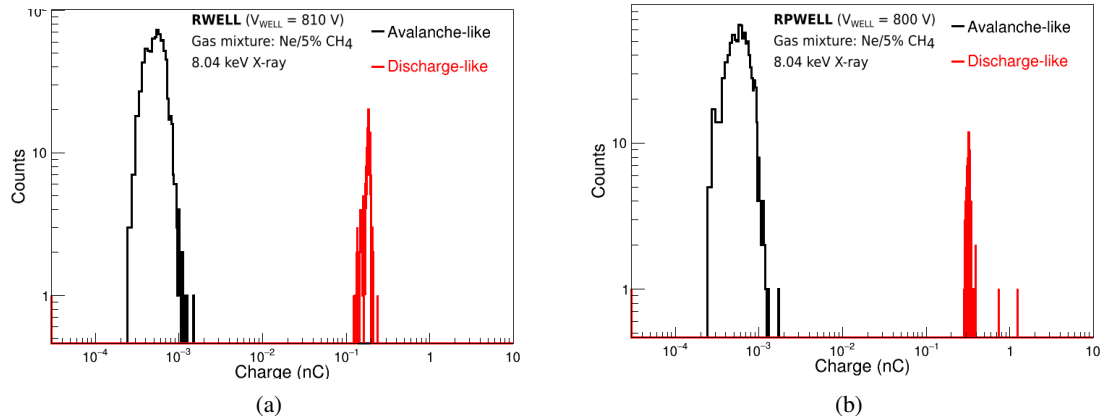


Figure 8: Charge distribution in avalanche and discharge-like events calculated from (a) RWELL pulses at $V_{WELL} = 810$ V, (b) RPWELL pulses at $V_{WELL} = 800$ V (pulse acquisition using TFA with 20 ns integration time).

are observed in all the three detectors in their proportional operation mode. Due to the limited

sensitivity of the TFA, only the high charge tail of the avalanche-like pulses could be measured, of the order of hundreds of fC. The second population (red curve) corresponds to the charge induced on the readout anode in a discharge event. Its typical magnitude is of the order of hundreds of pC.

The largest avalanches (pulses of ~ 100 fC charge) consist of about 10^7 electrons, in agreement with the reported Raether limit [1]. These direct measurement of the Raether limit in WELL-based configurations strengthens the claim according to which the large-amplitude pulses are induced by discharges. In the following, discharge-like events are selected by setting a 70 pC threshold.

The distribution of the charge induced on the readout anode in discharge-like pulses is shown in figure 9a for the RWELL (blue curve) and RPWELL (red curve). The charge estimated from the peaks of the current supplied to the Well-top electrode in the THWELL (black curve) and RWELL (green curve) are also shown. In all configurations, the measurements were taken at a gain of around 10^4 . The mean of the Gaussian fit of these distributions are shown as a function of the equivalent detector gain in figure 9b along with their respective errors found from the fit. Several

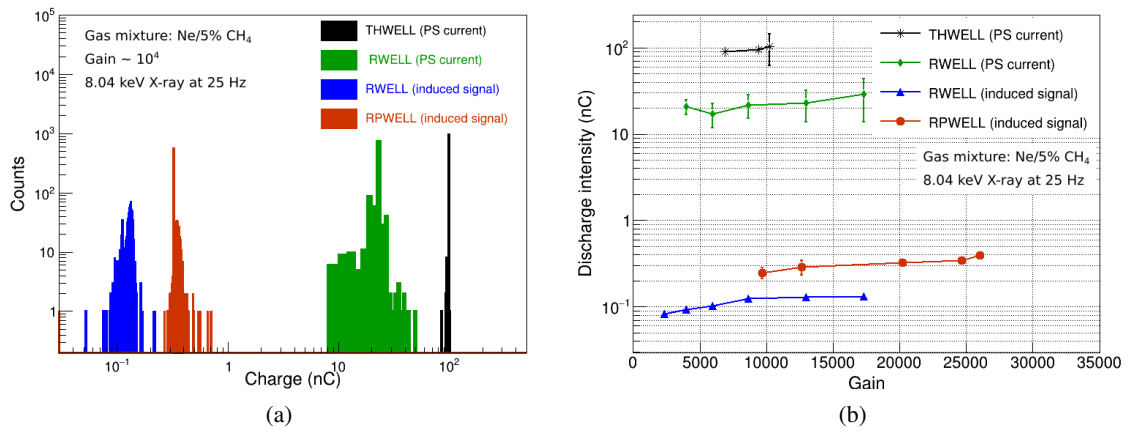


Figure 9: (a) Distribution of discharge intensity for the three investigated detectors. The bias voltage and the gain of the three detectors for this plot are: THWELL (745 V, $G = 9.5 \times 10^3$), RWELL (810 V, $G = 1.3 \times 10^4$), RPWELL (800 V, $G = 2 \times 10^4$), (b) variation of discharge intensity with the gain of the three investigated detectors at a source rate of 25 Hz.

observations can be made. For all the tested configurations, the discharge intensity (measured charge) has a very small dependency on the effective gain. The energy released in the discharge of a THWELL is an order of magnitude larger than that released in the discharge of an RWELL. For the latter, the charge measured on the anode (induced pulses) is two orders of magnitude smaller than that measured on the Well-top (power supply current). This large difference suggests that these quantities are governed by two different physics processes. The charge estimated from the current supply corresponds to the discharge of the equivalent Well-top/resistive layer capacitor. The current in this case flows through a conductive path between the Well-top and the resistive layer and, thus, do not induce signal on the anode. The charge measured on the anode could be induced by the large amount of charges moving in the gaseous medium before the streamer connects the Well-top and the resistive layer. This amount should not change much for the RWELL and RPWELL configurations. Nonetheless, due to the addition of the 0.9 mm thick insulator, the signal induced underneath the

resistive layer is reduced (as discussed in 2.3). In both cases, the resistive component decouples the anode from the intense discharge of the equivalent capacitor. For the THWELL, this is not the case and the charge released in the discharge of the equivalent capacitor overwhelms any other phenomenon.

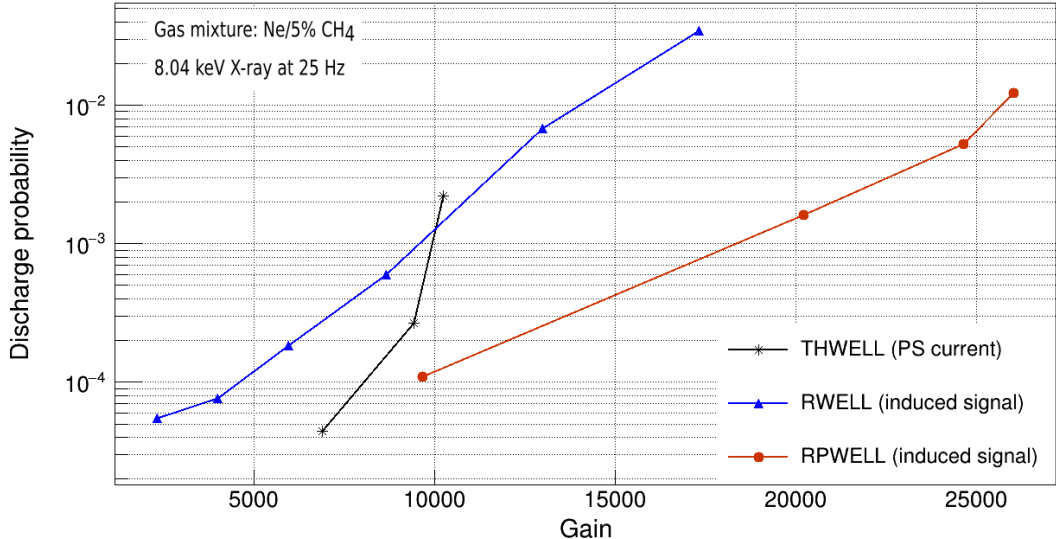


Figure 10: Variation of discharge probability with the gain of the three investigated detectors at a source rate of 25 Hz.

The discharge probability as a function of the detector gain for the three detectors is shown in figure 10. While the discharge probability rise quickly and roughly at the same gain for both the THWELL and RWELL, it rises slower for the RPWELL. Given the low event rate, the possibility of gain drop due to a single discharge being the reason for suppression of consequent discharges in RPWELL is excluded, suggesting that another mechanism could mitigate the occurrence of discharges in this configuration. The detectors could not be operated with discharge probability above ~ 0.02 . This corresponds to gain values of about 10^4 , 1.7×10^4 and 2.6×10^4 for the THWELL, RWELL and RPWELL, respectively.

4 Summary

In this paper, we have shown that discharges occur in WELL-based detectors with and without resistive anodes. Nonetheless, they take different forms in different configurations and consequently they have different effects on the detector performance.

In the case of the non-resistive WELL variant (THWELL), once the Raether limit is crossed and the gas breaks down, a direct conductive path is formed between the Well-top and the anode (ground), resulting in an intense discharge of the energy stored between the two. Indeed, in this scenario, no current was measured on the cathode while large currents of similar magnitude and opposite polarity were measured on the Well-top and the anode. These violent discharges limit the voltage that can be applied to the detector, its gain and eventual dynamic range.

In the RWELL and RPWELL configurations, there is no direct path between the Well-top and the ground. Instead, the electrons are forced to flow through a resistive path. The resistances seen by the evacuating charges are about $16\text{ M}\Omega$ and hundreds of $\text{G}\Omega$ for the RWELL and RPWELL (see appendix A), respectively. The slow charge evacuation via the resistive path decreases the effective electric field locally. As a result, the energy released in a discharge in RWELL is reduced by an order of magnitude. The discharge intensity in the investigated RWELL and RPWELL prototypes were found to be five times and hundred times lower than the non-resistive THWELL detector. Similar to the THWELL scenario, no current was measured on the RWELL cathode. Currents of opposite polarity were measured on the Well-top and the resistive layer. This was accompanied by synchronized appearance of large pulses on the anode. These pulses have two orders of magnitude higher amplitude than those at normal operating condition. Similar to RWELL, occurrence of discharges in RPWELL induce large pulses on its anode. This is accompanied by small current fluctuations on the Well-top, below the 5 nA sensitivity of the recording instrument. In this case also, no current was measured on the cathode.

The standard discharge identification method by monitoring electrode currents works when the gas breakdown is followed by discharge of a capacitor involving the electrodes. In detectors with resistive anode where the readout is shielded from the gaseous medium (e.g. in case of RPWELL, RPC [34] and other resistive gaseous detectors) gas breakdown induces large pulses on the readout, but no current may be detected by standard current monitoring devices. The newly presented method will be helpful in identifying gas breakdown in such cases.

A RPWELL gain curves at different source rates

Variation of effective gain of RPWELL as a function of voltage measured at different source rates is shown in figure 11a. The quoted values of rate are taken from the MCA acquisition rate.

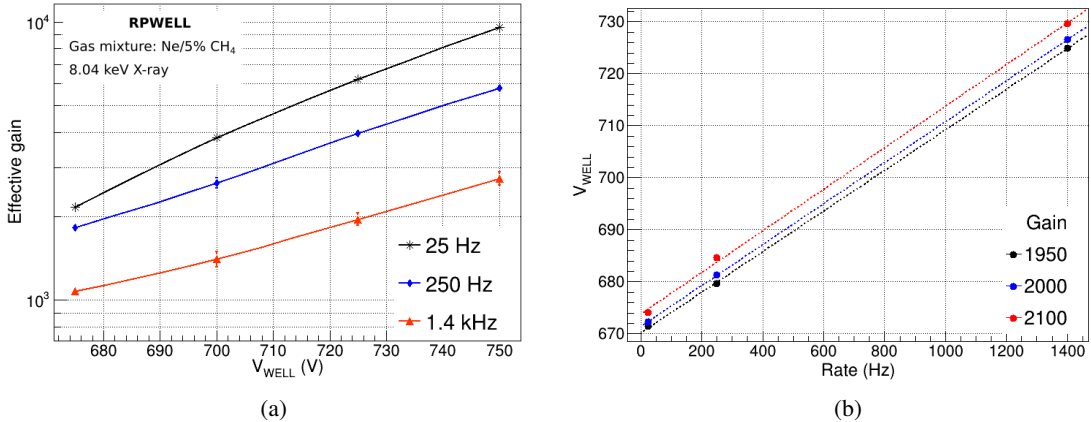


Figure 11: (a) Variation of effective gain of RPWELL with the applied voltage at different source rates, (b) plot of required voltage vs source rate to achieve a fixed gain from RPWELL.

Starting with Q_0 primary charge, the total charge produced per unit time after an avalanche (at the pit of RPWELL hole) is $r \times Q_0 \times G$, where r is the primary event rate and G is the effective

gain of the detector. Evacuation of this charge through the bulk of the resistive plate creates a voltage drop across it, in opposite direction to the applied bias producing an effective voltage, $V_{eff} = V_{WELL} - R \times r \times Q_0 \times G$, where R is the glass resistance faced by the evacuating charges. The electron avalanche at the RPWELL holes and consequently the gain of the detector depends on the field produced by this V_{eff} . Higher the source rate, lower is V_{eff} giving rise to lower gain. Based on this understanding the gain curves of figure 11a were used to estimate the resistance of the glass plate, as described below and compared with the measured value.

The voltages required to have a fixed RPWELL gain at different source rates, as plotted in figure 11b are computed from a third order polynomial fit of the gain curves of figure 11a for the gain values in the range of 1950 - 2100. Each V_{WELL} vs Rate curve is fit with a straight line. The slope of each fit is used to find the effective resistance offered by the glass plate according to the formula,

$$R = \frac{\Delta V_{WELL}/\Delta r}{Q_0 \times G}$$

The value of the calculated resistance was found to be around $520 \text{ G}\Omega$ which falls in the region of expected value of resistance for participation of a single hole ($700 \text{ G}\Omega$) or two holes ($350 \text{ G}\Omega$) in the charge evacuation process. The underlying assumption is that the glass area participating in charge evacuation equals the area of the holes where the charges are deposited.

Acknowledgments

This work was supported by Grant No. 3177/19 from the Israeli Science Foundation (ISF), The Pazy Foundation, and by the Sir Charles Clore Prize. We are grateful to Prof. Amos Breskin, Dr. David Vartsky, Dan Shaked Renous, Andrea Tesi and Darina Zavazieva for the helpful discussions and suggestions during this work.

References

- [1] H. Raether, *Electron Avalanches and Breakdown in Gases*, Butterworths, London (1964).
- [2] G. Battistoni et al., *Influence of gas mixture and cathode material on limited streamer operation*, *Nucl. Instrum. Meth. A* 217 (1983) 433.
- [3] F.E. Taylor, *A model of the limited streamer mechanism*, *Nucl. Instrum. Meth. A* 289 (1990) 283.
- [4] A. Bressan et al., *High rate behavior and discharge limits in micropattern detectors*, *Nucl. Instrum. Meth. A* 424 (1999) 321.
- [5] G. Charles et al., *Discharge studies in MicroMegas detectors in low energy hadron beams*, *Nucl. Instrum. Meth. A* 648 (2011) 174.
- [6] S. Bachmann et al., *Discharge studies and prevention in the gas electron multiplier (GEM)*, *Nucl. Instrum. Meth. A* 479 (2002) 294.
- [7] T.Alexopoulos et al., *A spark-resistant bulk-micromegas chamber for high-rate applications*, *Nucl. Instrum. Meth. A* 640 (2011) 110.
- [8] A. Di Mauro et al., *Development of innovative micro-pattern gaseous detectors with resistive electrodes and first results of their applications*, *Nucl. Instrum. Meth. A* 581 (2007) 225.

- [9] R. Santonico and R. Cardarelli, *Development of resistive plate counters*, *Nucl. Instr. Meth. A* 187 (1981) 377.
- [10] L. Arazi, M. Pitt, S. Bressler, L. Moleri, A. Rubin and A. Breskin, *Laboratory studies of THGEM-based WELL structures with resistive anode*, *JINST* 9 (2014) P04011.
- [11] L. Arazi, M. Pitt, S. Bressler, L. Moleri, A. Rubin and A. Breskin, *THGEM-based detectors for sampling elements in DHCAL: laboratory and beam evaluation*, *JINST* 7 (2012) C05011.
- [12] A. Rubin et al., *First studies with the Resistive-Plate WELL gaseous multiplier*, *JINST* 8 (2013) P11004.
- [13] R. Chechik et al., *Thick GEM-like hole multipliers: properties and possible applications*, *Nucl. Instrum. Meth. A* 535 (2004) 303.
- [14] A. Breskin et al., *A concise review on THGEM detectors*, *Nucl. Instrum. Meth. A* 598 (2009) 107.
- [15] F. Sauli, *The gas electron multiplier (GEM): Operating principles and applications*, *Nucl. Instr. Meth. A* 805 (2016) 2-24.
- [16] M. Pitt et al., *Measurements of charging-up processes in THGEM-based particle detectors*, *JINST* 13 (2018) P03009.
- [17] D. Shaked Renous et al., *Gain stabilization in Micro Pattern Gaseous Detectors: methodology and results*, *JINST* 12 (2017) P09036.
- [18] M. Cortesi et al., *Investigations of a THGEM-based imaging detector*, *JINST* 2 (2007) P09002.
- [19] L. Moleri et al., *On the localization properties of an RPWELL gas-avalanche detector*, *JINST* 12 (2017) P10017.
- [20] R. Alon, M. Cortesi, A. Breskin and R. Chechik, *Time resolution of a Thick Gas Electron Multiplier (THGEM)-based detector*, *JINST* 3 (2008) P11001 [arXiv:0809.4382].
- [21] C. Shalem et al., *Advances in Thick GEM-like gaseous electron multipliers—Part I: atmospheric pressure operation*, *Nucl. Instrum. Meth. A* 558 (2006) 475.
- [22] R. Chechik and A. Breskin, *Advances in gaseous photomultipliers*, *Nucl. Instrum. Meth. A* 595 (2008) 116 [arXiv:0807.2086].
- [23] S. Bressler et al., *Novel Resistive-Plate WELL sampling element for (S)DHCAL*, *Nucl. Instr. Meth. A* 958 (2020) 162861.
- [24] L. Arazi et al., *Laboratory studies of THGEM-based WELL structures with resistive anode*, figure 4, *JINST* 9 (2014) P04011.
- [25] L. Moleri et. al, *The Resistive-Plate WELL with Argon mixtures - A robust gaseous radiation detector*, *Nucl. Instr. Meth. A* 845 (2017) 262.
- [26] S. Bressler et. al, *First in-beam studies of a Resistive-Plate WELL gaseous multiplier*, *JINST* 11 (2016) P01005.
- [27] S. Bressler et. al, *Recent advances with THGEM detectors*, *JINST* 8 (2013) C12012.
- [28] J. Wang et al., *Development of multi-gap resistive plate chambers with low-resistive silicate glass electrodes for operation at high particle fluxes and large transported charges*, *Nucl. Instrum. Meth. A* 621 (2010) 151.
- [29] I.B. Smirnov, *Modeling of ionization produced by fast charged particles in gases*, *Nucl. Instr. Meth. A* 554 (2005) 474.

- [30] W. Shockley, *Currents to conductors induced by a moving point charge*, *J. Appl. Phys.* 9 (1938) 635.
- [31] S. Ramo, *Currents induced by electron motion*, *Proc. IRE* 27 (1939) 584.
- [32] P. Bhattacharya et al., *Signal formation in THGEM-like detectors*, *Nucl. Instr. Meth. A* 916 (2019) 125.
- [33] L. Moleri et al., *A detector-emulation method for realistic readout-electronics tests. A case study of VMM3a ASIC for sTGC detector*, *JINST* 17 (2022) P02037.
- [34] R. Cardarelli et al., *Avalanche and streamer mode operation of resistive plate chambers*, *Nucl. Instr. Meth. A* 382 (1996) 470.